Microstructure characterization and hydrogen permeation study of high strength steels

Darya NOVIKOVA[1], Tomáš PROŠEK[2], Andreas MUHR[3], Hubert DUCHACZEK[4], Gerald LUCKENDER[5], Gabriela SCHIMO[6], Pavel NOVÁK[7], Pavel SALVETR[8]

[1] University of Chemistry and Technology Prague, Czech Republic, novikovr@vscht.cz
[2] University of Chemistry and Technology Prague, Czech Republic, prosekt@vscht.cz
[3] voestalpine Stahl GmbH, Linz, Austria, Andreas.Muhr@voestalpine.com
[4] voestalpine Stahl GmbH, Linz, Austria, Hubert.Duchaczek@voestalpine.com
[5] voestalpine Stahl GmbH, Linz, Austria, Gerald.Luckeneder@voestalpine.com
[6] CEST Kompetenzzentrum für elektrochemische Oberflächentechnologie GmbH, W. Neustadt, Austria, gabriela.schimo@cest.at
[7] University of Chemistry and Technology Prague, Czech Republic, panovak@vscht.cz
[8] University of Chemistry and Technology Prague, Czech Republic, pavel.salvetr@vscht.cz

Abstract:

Hydrogen embrittlement of high strength steels is a subject of intense study in recent years. However, hydrogen effects on HSSs in the micro-scale have not been investigated carefully enough. Scanning Kelvin Probe Atomic Microscopy is one of the promising techniques with very high spatial resolution to study the influence of particular phases on the hydrogen embrittlement process. Precise characterization of steel microstructure is a necessary step before following experiments with SKPFM. Microstructures of two types of advanced high strength steels (AHSS) have been investigated in this work. Hydrogen permeation tests were carried out to compare hydrogen permeability in complex phase (CP) and dual phase (DP) AHSS.

Keywords: high strength steel, hydrogen diffusion, microstructure characterization, permeability.

Introduction

Demand for lighter and more fuel efficient vehicle have led to development of high strength steels. Advanced high strength steels (AHSS) are steels with multiphase microstructure and tensile strength level in excess of 600 MPa. The coexistence of phases provides improved mechanical properties such as high tensile strength and high elongation. This favourable combination of mechanical properties is achieved by chemical composition of the steel and specific heat treatment. There are four main classes of AHSSs: dual phase (DP) steels, complex phase (CP) steels, transformation-induced plasticity steels (TRIPs) and martensitic steels with different microstructure depending on their final purpose. Representatives of DP and CP classes were studied in this paper.

DP steels have a microstructure of a soft ferrite matrix with hard martensite islands. These steels have very good combination of formability and strength characteristics as low yield strength and relatively high ultimate tensile strength. DP steels are produced by intercritical annealing, followed by a very rapid cooling to transform the austenite to martensite. The carbon content has the most significant influence on properties of DP steels [1]. Other alloying elements as Mn, Si, Cr, Mo, V and Nb contributes to strengthening or regulation of the phase transformation rate.

CP steels have a very fine ferrite-bainite matrix with small amounts of martensite, retained austenite and pearlite fractions. In comparison with DP steels, CP steels have higher yield strength at equal strength levels [2]. Specific heat treatment includes annealing, cooling to temperature below bainite start temperature and holding at this temperature, followed by final cooling.

With a growing interest in AHSSs, issue of their susceptibility to hydrogen embrittlement becomes more investigated. In literature, steels with tensile strength higher than 1000 MPa are often said to be susceptible for hydrogen embrittlement (HE). Contamination of steel by hydrogen may originate from steel production and fabrication but also absorption of hydrogen may occur during steel service as a result of the cathodic corrosion reaction. The content of hydrogen can be reduced after production steps by specific heat treatment, but HE as a consequence of corrosion may principally cause an unexpected failure.

It was found that a number of defects could be responsible for HE and grain/phase boundaries could serve as crack initiation sites in high strength steels [3-5]. Increasing carbon content in a DP steel led to growth of a martensite to ferrite fraction ratio [6]. Martensite replacement by granular bainite improved extrinsic resistance to HE due to decreasing number of trapping sites [7]. Austenite as a phase with higher hydrogen solubility can trap hydrogen and decrease HE as long as retained austenite is stable [8]. These observations suggest that research into correlations between microstructure features and processes related to HE would be of great interest.

Comparison of hydrogen diffusion properties in AHSSs with different microstructures is often provided by permeation measurements with electrochemical Devanathan-Stachurski cell [9-12]. It consists of two compartments separated by a thin metal sample that acts as a common working electrode. A cathodic polarization is applied in the first cell to promote hydrogen evolution on the sample surface. After absorption in monatomic form a proportion of hydrogen diffuses through the sample and is oxidized on the opposite surface of the sample. Diffusion of hydrogen in metal can be determined by the change in oxidation current measured between the sample and a counter electrode in the second cell. Diffusion

coefficient, concentration of trapped hydrogen and density of reversible traps may be calculated. However, this technique can assess only bulk properties.

There is a promising technique with high spatial resolution, which would allow following hydrogen permeation through grains of different phases or along grains boundaries [13]. It is the Scanning Kelvin Probe Force Microscopy (SKPFM). The Scanning Kelvin Probe (SKP) technique, measuring differences in Volta potential caused by hydrogen, showed good results in experiments with precharged samples [14] and with in-situ hydrogen loaded samples [15] of AHSSs. Thus, SKPFM with much better resolution than SKP may provide useful data in relation to steels microstructures [13, 16, 17]. At the same time, there is a need for precise structure characterization for correct interpretation of SKPFM measurements.

In this study, microstructure characterization of a CP steel and a DP steel was done before a forthcoming investigation of these steels with SKPFM. The permeation technique was used for determining of diffusion coefficients of the steels. Model structures with prevalence of martensite, bainite or ferrite phase were prepared for comparison with the original steels.

Experimental

Two types of AHSSs provided by voestalpine Stahl were studied: dual-phase grade DP1000 and complex-phase grade CP1000, both with ultimate tensile strength R_m 980 MPa.

Chemical composition of the samples was determined by Glow-Discharge Optical Emission Spectroscopy (GDOES), X-Ray Fluorescence (XRF) and Inductively Coupled Plasma Optical Emission Spectrometry (ICP-OES).

Following techniques were used for microstructure characterization of DP1000 and CP1000 steels: Neutron Diffraction (ND), X-Ray Diffraction (XRD), colour metallography, Scanning Electron Microscopy (SEM) and Transmission Electron Microscopy (TEM).

Simplified model structures for hydrogen diffusion experiments were prepared from DP1000 and CP1000 steel samples by heat treatment. Procedures of preparations are described in Table 2.

Table 2: Preparation of model structures

Model structure	Heat treatment
"Model Ferrite"	annealing at 950 °C for 30 min cooling in furnace
"Model Bainite"	annealing at 950 °C for 30 min cooling in heated oil (80 °C) for 10 min cooling at lab temperature
"Model Martensite"	annealing at 1050 °C for 30 min cooling in NaCl solution cooling in liquid nitrogen

Permeation measurements were performed in the Devanathan-Stachurski double electrolytic permeability cell. The schematic setup is illustrated in Figure 1. The cathodic side of the cell contained 0.5 M sulfuric acid solution with 40 mg l^{-1} thiourea as recombination poison. The anodic side of the cell was filled with 0.1 M sodium hydroxide solution. Steel samples were

electrochemically coated by Pd on the anodic side and nitrogen gas was bubbled through NaOH solution during all measurements to prevent oxidation. The current was recorded by polarizing the hydrogen exit side to 300 mV vs. SCE.

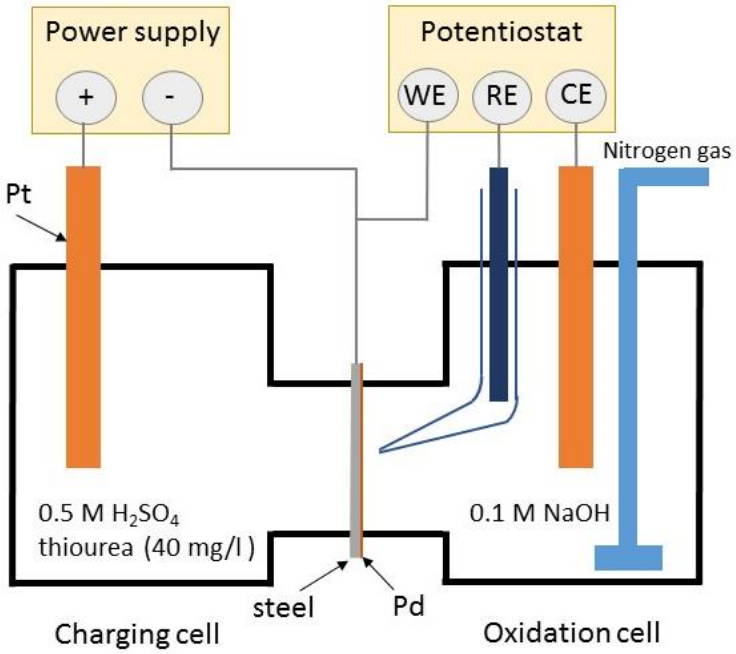

Figure 1: Permeation setup

Microstructure characterization

Detail characterization of phases presented in CP1000 and DP1000 AHSSs was performed in order to understand results of following experiments in terms of steel microstructure. Only content of austenite in both steels was assessed by XRD. ND allowed for defining lattice parameters of ferrite, martensite and austenite, to determinate the martensite content and to approve the austenite content. Based on the assumption that martensite should have a slightly greater lattice parameter than ferrite, the phase with parameter a=2.876 Å (for CP1000) and a=2.874 Å (for DP1000) was assumed to be martensite and the phase with a=2.866 Å as ferrite. The third phase with lattice parameter a=3.605 Å (CP1000) and a=3.602 Å (DP1000) was austenite. In the case of CP steel, it was impossible to distinguish bainite from ferrite, thus another technique was needed.

Colour metallography was the only technique to distinguish bainite from other phases in CP steels in this study. The CP steel samples were etched in 2 vol. % NITAL solution for 1 minute after mechanical polishing and studied with light microscope Olympus PME3. Bainite appeared as a blue phase, martensite was brown and ferrite and austenite were white [18]. The content of bainite was determined applying threshold technique in ImageJ software. The combined data on the phase structure of DP1000 and CP1000 steels are in Table 3.

Scanning electron microscope TESCAN VEGA 3 LMU was used for visual characterization of the steel microstructure after NITAL etching for topography contrast. Ferrite was the most etched phase due to smaller content of carbon and martensite was the least etched phase due to the highest carbon content. In the case of CP1000, martensite (marked ‘M’ in Figure 2) appeared as plate or polygonal grains with size 3–15 μm, ferrite (marked ‘F’) as polygonal grains with size 0.7–7 μm and bainite (marked ‘B’) as grains with size 1.6–10 μm and

characteristic laths. In DP1000, the martensite phase was continuous with individual grains with size 0.8–8 μm and ferrite was present in form of 1–5 μm polygonal grains.

Table 3: Phase composition of studied AHSSs

Phase	Phase fraction [%]		Technique
	CP1000	DP1000	
Martensite / temp. Martensite	47	62	Neutron diffraction
Ferrite	32	36	Neutron diffraction
Bainite	20	–	Colour metallography
Austenite	1	2–2.5	X-Ray Diffraction, neutron diffraction

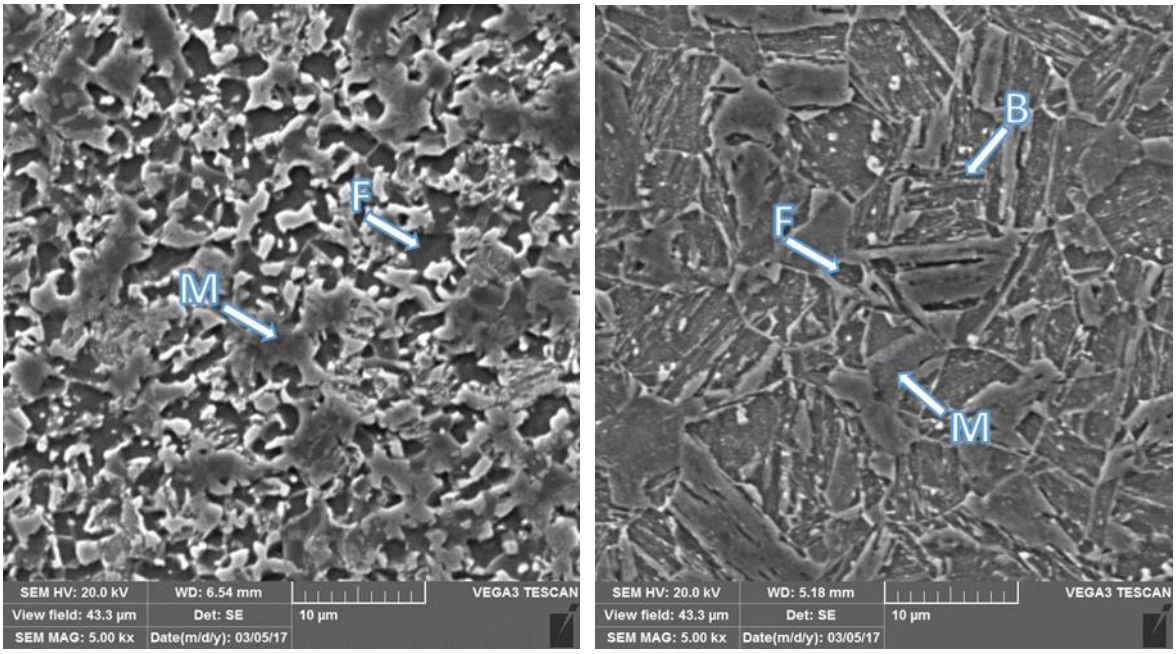

Figure 2: SEM images of DP1000 (left) and CP1000 (right).

Transmission electron microscope EFTEM Jeol 2200 FS was used for identification of small particles in steel phases and Energy Dispersive Spectrometry (EDS) was applied to define the chemical composition of the particles. The particles were observed mostly in the ferrite phase. In CP1000, there were Ti-V carbonitrides, Ti-V mixed carbides and Fe carbides (Figure 3). In DP1000, Mn carbides, Mn-Nb mixed carbides and Fe carbides were determined.

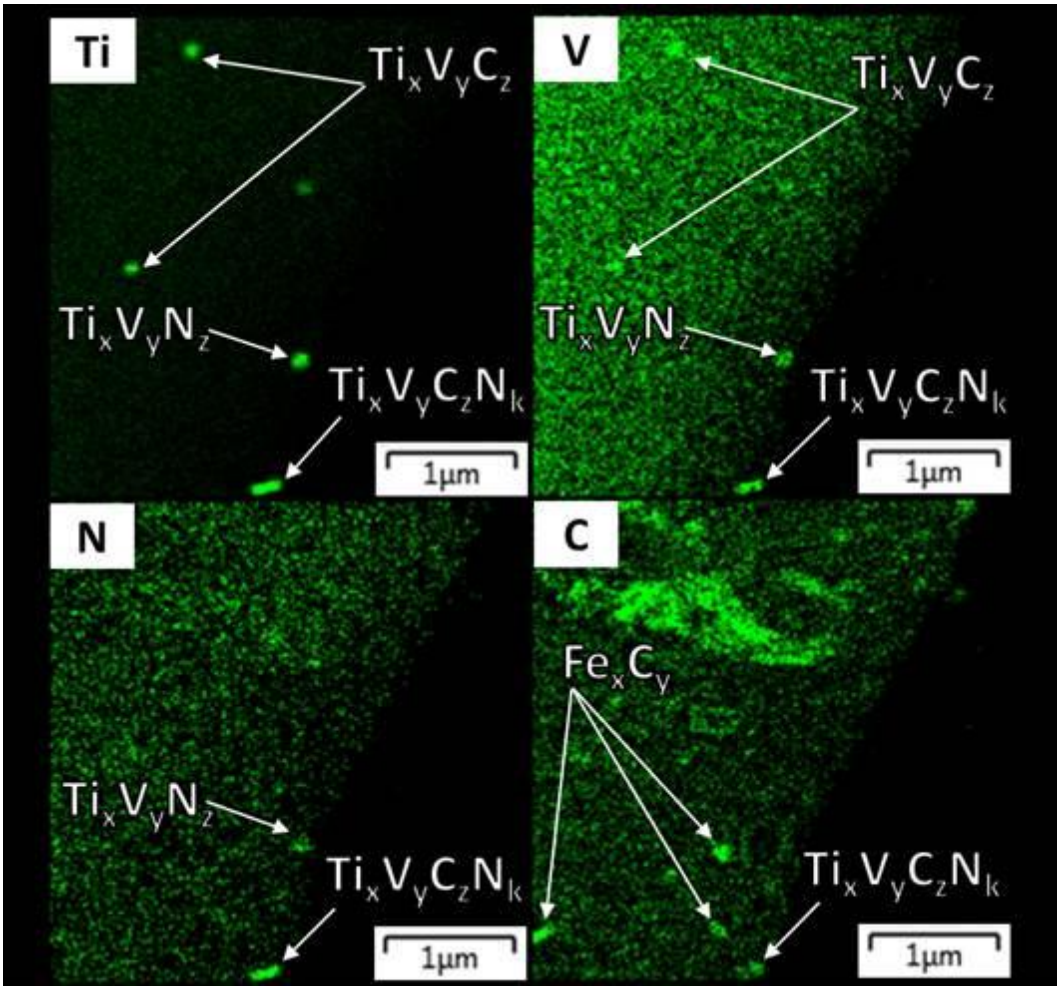

Figure 3: Micro particles identified in CP1000 by TEM EDS.

Martensite, bainite and ferrite phases were found in CP1000 steel after NITAL etching by measurements with atomic force microscope AIST-NT SmartSPM. The continuous ferrite matrix and grains of martensite were observed in DP1000 by the same way. This indicates that topography measurements can be used for phase determination by SKPFM.

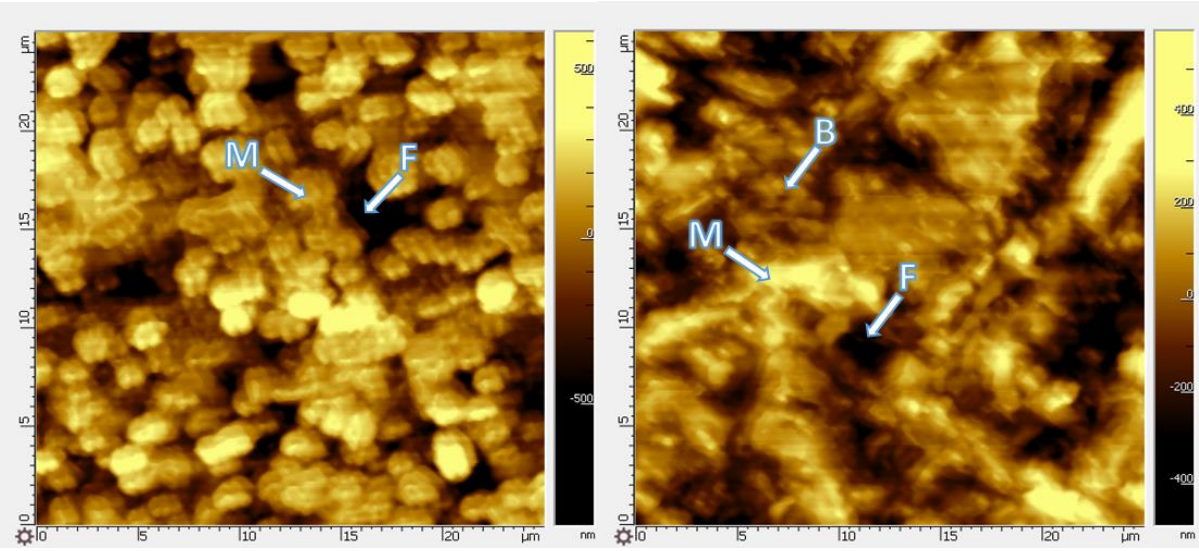

Figure 4: AFM topography images of DP1000 (left) and CP1000 (right).

Hydrogen permeation measurements

Permeation tests were conducted on CP1000 and DP1000 steels. Measurements on model phases are in progress. Diffusion coefficient values presented in Figure 5 were calculated using the time lag method in accordance with ISO 17081.

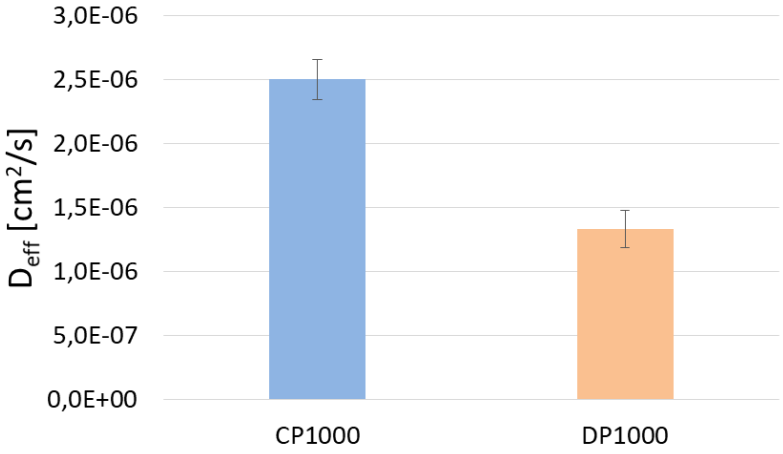

Figure 5: Diffusion coefficients of AHSSs

Hydrogen diffusion coefficient was also calculated by fitting of experimental permeation curves with theoretical curves according to the following equation:

$$i = i^0 + (i^\infty - i^0)\frac{2L}{\sqrt{\pi D t}}\sum_{n=0}^{\infty}\exp\left(-\frac{(2n+1)^2 L^2}{4Dt}\right)$$

where i is the measured permeation current density at time t, i^0 is the initial permeation current density, i^∞ is the steady-state permeation current density, L is the thickness of the steel membrane and D is the diffusion coefficient. An example of experimental and fitted curves is shown in Figure 6. Diffusion coefficients obtained using the two calculation methods were similar.

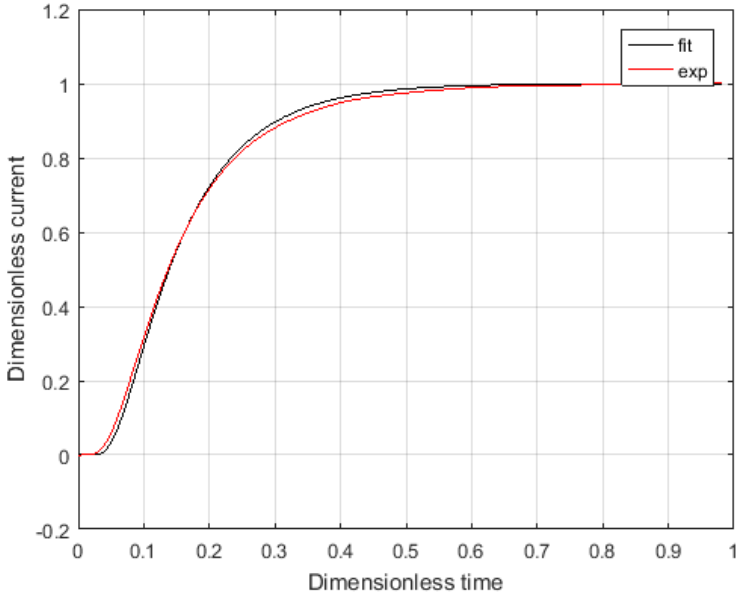

Figure 6: Experimental and fitted curves for CP1000 steel.

The hydrogen diffusion coefficient in CP1000 steel was almost two times higher than in DP1000 steel. The lower diffusion rate for DP1000 can be caused by a greater number of trapping sites, which retard transport of hydrogen atoms through the steel. DP1000 contains more martensite in comparison with CP1000. Martensite has high dislocation density and consequently high hydrogen-trapping capability [19]. Thus, an increase of the martensite content may lead to slower hydrogen diffusion.

Results of this study in view of the diffusion coefficient for DP1000 and the relationship between martensite content and the diffusion coefficient are consistent with data of Liu et al. [20]. They obtained a range of diffusion coefficients for DP steels from $0.51 \cdot 10^{-6}$ cm^2 s^{-1} to $1.25 \cdot 10^{-6}$ cm^2 s^{-1}. Hydrogen diffusion coefficient values decreased with the increasing martensite content in DP steels and increasing yield strength and tensile strength parameters. Hadzipasic et al. measured diffusion coefficient of $0.7 \cdot 10^{-6}$ cm^2 s^{-1} for DP steel of approximately 600 MPa tensile strength [21], which is also close to results of this study. Rehrl et al. [22][23] found that diffusion coefficient of CP1200 was slightly lower in comparison with DP1200. No other measurements for CP steels have been published.

Conclusions

1. Microstructure characterization of DP1000 and CP1000 steels was carried out. Volume fractions, size and distribution of ferrite, martensite, bainite and austenite were determined. Particles as carbides, nitrides and carbonitrides of alloying elements and iron were found in ferrite phases.
2. Hydrogen diffusion coefficient for DP1000 and CP1000 was $1.3 \cdot 10^{-6}$ cm^2 s^{-1} and $2.5 \cdot 10^{-6}$ cm^2 s^{-1}, respectively. Hydrogen permeability measurements with model steels with prevalence of particular phases are in progress.
3. Obtained data support further micro scale measurements on DP1000, CP1000 and model structures with SKPFM.

Acknowledgements

A part of this research was financially supported by the Czech Science Foundation, project No. 17-22586S.

References

1. El-Sesy, I.A. and Z.M. El-Baradie, *Influence carbon and/or iron carbide on the structure and properties of dual-phase steels.* Materials Letters, 2002. **57**(3): p. 580-585.
2. Hofmann, H., D. Mattissen, and T.W. Schaumann, *Advanced Cold Rolled Steels for Automotive Applications.* Steel Research International, 2009. **80**(1): p. 22-28.
3. Zhu, X., et al., *Hydrogen trapping sites and hydrogen-induced cracking in high strength quenching & partitioning (Q&P) treated steel.* International Journal of Hydrogen Energy, 2014. **39**(24): p. 13031-13040.
4. Koyama, M., et al., *Hydrogen-induced cracking at grain and twin boundaries in an Fe-Mn-C austenitic steel.* Scripta Materialia, 2012. **66**(7): p. 459-462.
5. Ishikawa, N., H. Sueyoshi, and A. Nagao, *Hydrogen Microprint Analysis on the Effect of Dislocations on Grain Boundary Hydrogen Distribution in Steels.* Isij International, 2016. **56**(3): p. 413-417.
6. Davies, R.G., *Influence of Martensite Content on the Hydrogen Embrittlement of Dual-Phase Steels.* Scripta Metallurgica, 1983. **17**(7): p. 889-892.
7. Shim, D.H., et al., *Increased resistance to hydrogen embrittlement in high-strength steels composed of granular bainite.* Materials Science and Engineering a-Structural Materials Properties Microstructure and Processing, 2017. **In Press**.
8. Yang, J., et al., *Effect of retained austenite on the hydrogen embrittlement of a medium carbon quenching and partitioning steel with refined microstructure.* Materials Science and Engineering: A, 2016. **665**: p. 76-85.
9. Frappart, S., et al., *Study of the hydrogen diffusion and segregation into Fe-C-Mo martensitic HSLA steel using electrochemical permeation test.* Journal of Physics and Chemistry of Solids, 2010. **71**(10): p. 1467-1479.
10. Winzer, N., et al., *Hydrogen diffusion and trapping in Ti-modified advanced high strength steels.* Materials & Design, 2016. **92**: p. 450-461.
11. Hu, Y., et al., *Study on the Hydrogen Embrittlement of Aermet100 Using Hydrogen Permeation and SSRT Techniques.* Metallurgical and Materials Transactions A, 2017. **In Press**: p. 1-12.
12. Kim, S.J. and K.Y. Kim, *Electrochemical hydrogen permeation measurement through high-strength steel under uniaxial tensile stress in plastic range.* Scripta Materialia, 2012. **66**(12): p. 1069-1072.
13. Evers, S., C. Senöz, and M. Rohwerder, *Spatially resolved high sensitive measurement of hydrogen permeation by scanning Kelvin probe microscopy.* Electrochimica Acta, 2013. **110**: p. 534-538.
14. Nazarov, A.P., A.I. Marshakov, and A.A. Rybkina, *Iron hydrogenation under atmospheric corrosion. Studies using a scanning vibrating microscope.* Protection of Metals and Physical Chemistry of Surfaces, 2015. **51**(3): p. 347-359.
15. Nazarov, A., F. Vucko, and D. Thierry, *Scanning Kelvin Probe for detection of the hydrogen induced by atmospheric corrosion of ultra-high strength steel.* Electrochimica Acta, 2016. **216**: p. 130-139.

16. Senöz, C., et al., *Scanning Kelvin Probe as a highly sensitive tool for detecting hydrogen permeation with high local resolution.* Electrochemistry Communications, 2011. **13**(12): p. 1542-1545.
17. Wang, G., et al., *Investigation of hydrogen evolution and enrichment by scanning Kelvin probe force microscopy.* Electrochemistry Communications, 2013. **35**: p. 100-103.
18. Zakerinia, H., A. Kermanpur, and A. Najafizadeh, *Color metalography; a suitable method for characterization of martensite and bainite in multiphase steels.* International Journal of ISSI, 2009. **6**(1): p. 14-18.
19. Koyama, M., et al., *Hydrogen-assisted decohesion and localized plasticity in dual-phase steel.* Acta Materialia, 2014. **70**: p. 174-187.
20. Liu, Q., et al., *Hydrogen trapping in some advanced high strength steels.* Corrosion Science, 2016. **111**: p. 770-785.
21. Hazipasic, A.B., J. Malina, and S. Niznik, *The Influence of Microstructure on Hydrogen Diffusion and Embrittlement of Multiphase Fine-Grained Steels with Increased Plasticity and Strength.* Chemical and Biochemical Engineering Quarterly, 2011. **25**(2): p. 159-169.
22. J. Rehrl, K. Mraczek, A. Pichler and E.Werner, *The Impact of Nb, Ti, Zr, B, V, and Mo on the Hydrogen Diffusion in Four Different AHSS/UHSS Microstructures.* Steel Research International, 2014. **85**(3): p. 336-346.
23. J. Rehrl, K. Mraczek, A. Pichler, and E. Werner (2014). *Mechanical properties and fracture behavior of hydrogen charged AHSS/UHSS grades at high-and low strain rate tests.* Materials Science and Engineering: A, 590, 360-367.